Raab, T., Reinsch, T., Aldaz Cifuentes, S. R., Henninges, J. (2019): Real-Time Well-Integrity Monitoring Using Fiber-Optic Distributed Acoustic Sensing. - *SPE Journal*, *24*, 05, pp. 1997—2009.

DOI: http://doi.org/10.2118/195678-PA

Real-Time Well Integrity Monitoring using Fiber-Optic Distributed Acoustic Sensing

T. Raab, GFZ German Research Centre for Geosciences;
T. Reinsch, GFZ German Research Centre for Geosciences, Delft University of Technology;
S. R. Aldaz Cifuentes, and **J. Henninges**, GFZ German Research Centre for Geosciences

Summary

Proper cemented casing strings is a key requirement for maintaining well integrity therefore guaranteeing the optimal operation and safe provision of hydrocarbon and geothermal resources from the pay zone to surface facilities. Throughout the life cycle of a well, high temperature and pressure changes in addition to shut-in cyclic periods can lead to strong variations in thermal and mechanical load onto the well architecture. The current procedures to evaluate cement quality and to measure downhole temperature are mainly based on wireline logging campaigns. In this paper we investigate the application of the fiber-optic distributed acoustic sensing (DAS) technology to acquire dynamic axial strain changes caused by acoustic signals propagation along the wellbore structure. The signals are recorded by a permanently installed fiber-optic cable and studied for the possibility of real-time well integrity monitoring.

The fiber-optic cable was installed along the 18 5/8-in. anchor casing and the 21-in. hole section of a geothermal well in Iceland. During cementing operations, temperature was continuously measured using distributed temperature sensing (DTS) technology to monitor the cement placement. DAS data was acquired continuously for 9 days during drilling and injection testing of the reservoir interval in the 12 1/4-in open hole section. The DAS data was used to calculate average axial strain-rate profiles during different operations on the drill site. Signals recorded along the optical fiber result from elastic deformation due to mechanical energy applied from inside- (e.g. pressure fluctuations, drilling activities) or outside (e.g. seismic signals) of the well. The results indicate, that average axial strain-rate of a fiber-optic cable installed behind a casing string generates similar trends as a conventional cement bond log (CBL). The obtained trends along well depth therefore indicate that DAS data acquired during different drilling and testing operations can be used to monitor the mechanical coupling between cemented casing strings and the surrounding formations, hence the cement integrity. Potential DTS and DAS technology use in downhole evaluations would extend the portfolio to monitor and evaluate qualitatively in real-time cement integrity changes without the necessity of executing costly well intervention programs throughout the wells life cycle.

Introduction

Well integrity, according to ISO/TS 16530-2 (2014) defined as the containment and prevention of the escape of fluids (i.e. liquids or gases) to subterranean formations or surface, relies on adequate cementation of the casing strings. For wells drilled in high temperature and pressure regimes, e.g. high temperature geothermal wells, large cyclic load changes during drilling, well testing, fluid production or injection and shut-in periods occur. Cyclic load changes are known to cause a high risk of well failure (e.g. Goodwin and Crook 1992; Thiercelin et al. 1998; Southon 2005). In addition, recent studies indicate that the ability of the cement sheet to provide a mechanical seal against fluid migration deteriorates over time (e.g. Jackson 2014; Davies et al. 2014). To implement a modern cement state downhole monitoring system in the sustainable operation of subsurface reservoirs for production or injection of hydrocarbons and geothermal fluids, a passive real-time monitoring system with the incorporation of optical fibers will be discussed in this study.

Conventional Cement Evaluation Tools

Introduced in the late 50s by Grosmangin et al. (1961) as cement bond log (CBL), various implementations of sonic and ultrasonic source and receiver geometries are currently in use to evaluate the properties of the cemented annulus behind casing. Data acquisition and analysis relies on the signal propagation between source and receiver and its interaction with wellbore fluid, casing, cement and formation. The signals are among others influenced by the shear

modulus between casing and cement, the volume of cement behind casing and its mechanical properties, the impedance contrast between casing and cement as well as tool centralization (Pardue et al. 1963; Jutten et al. 1989; Song et al. 2013).

Fiber-Optic Sensing

In addition to conventional electronic sensors, fiber-optic based sensing systems have been increasingly used in downhole applications. With the advent of the distributed temperature sensing (DTS) technology (Hartog and Leach 1985), distributed sensing systems were increasingly used for e.g. geothermal studies (e.g. Hurtig et al. 1993; Förster et al. 1997). The optical fiber, embedded in a cable structure, acts as the sensing element. Interrogated with a read-out unit at the surface, temperature data can be retrieved with high temporal and spatial resolution along the entire length of the fiber. The fact that only the measurement cable is subject to potentially hostile downhole conditions, makes such fiber-optic systems suitable for operation in high temperature environments (e.g. Reinsch and Henninges 2010; Reinsch et al. 2013). In addition to DTS, techniques to detect and localize dynamic strain changes along an optical fiber have drawn attention over the last years. This technology is often referred to as distributed acoustic sensing (DAS). DAS has demonstrated its applicability to detect dynamic strain changes in a number of applications e.g. vertical seismic profiling (Daley et al. 2013; Götz et al. 2018), flow profiling (Bukhamsin and Horne 2016), near-surface geophysics (Dou et al. 2017), and seismology (Jousset et al. 2018). Measured strain changes are influenced by the coupling between the optical fiber and the medium the cable is installed in (e.g. Daley et al. 2013; Reinsch et al. 2017).

Both technologies (DTS and DAS) typically utilize an incident laser pulse and analyze of back-scattered light from individual points along the optical fiber. DTS systems mostly use the temperature sensitive Raman scattering (Dakin et al. 1985). DAS systems are commonly based on the detection of phase changes of Rayleigh back-scattered light (Hartog 2017). A change in the phase difference of light (between individual laser pulses) scattered by two separate points along the fiber is linear proportional to a change in fiber length separating the points (Masoudi et al. 2013). Determining these phase changes for consecutive fiber intervals and over time can therefore be used to record the dynamic strain evolution (strain-rate) of a fiber-optic cable induced e.g. by a seismic signal.

To determine the dynamic phase difference, a number of optical architectures have been proposed and used (see e.g. Liu et al. 2016, for a summery). For the presented study, the DAS interrogator unit sends short, coherent light pulses into the optical fiber. The phase difference is determined by splitting the back-scattered signal and feeding one part through an extra length of fiber (imbalanced Mach-Zehnder interferometer). The two signals are brought to interference. The measured intensity is therefore proportional to the phase difference between points separated by the length of the delay fiber, generally referred to as the gauge-length (Masoudi et al. 2013). For seismic applications, the gauge-length is in the order of 10 m (e.g. Jousset et al. 2018). Applying a dynamic force on a section of the fiber results in local length changes (strain ε), and therefore the measured phase difference. Comparing the phase differences between consecutive laser pulses provides, for a single DAS channel, an estimate of the dynamic strain evolution with time $\partial\varepsilon/\partial t$ of that fiber section. Modern DAS interrogator units are capable of extracting distributed acoustic data over several kilometers of fiber with sub-meter channel spacing (Parker et al. 2014).

In this study, we investigate the application of the DAS technology along a fiber-optic cable permanently installed behind the anchor casing of a high temperature geothermal well. Fibre optic acoustic data, acquired during drilling and testing the reservoir interval, together with fiber-optic DTS data will be used to qualitatively evaluate properties of the cement condition behind casing.

Field Deployment

Drilling Information and Cable Installation The fiber-optic cable was installed behind the 355-m 18-5/8 in. anchor casing of well RN-34 located in the Reykjanes geothermal field in Iceland **(Fig 1).** All depth specifications in this paper will be given in measured depth (MD) with reference to the ground level (GLV); the cellar reference level is set at 3 meters below GLV. The installed cable contains two single mode (SM1, SM2) and one multi mode (MM) fiber in a gel filled metal tube.

While the casing was run in hole, the cable was fixed to it using metal straps. During installation, the cable was damaged at approximately 175 m depth.

Recording data from the MM as well as the SM2 fiber was impossible below this point. Fibre SM1 was damaged as well but data acquisition was still possible to 217 m distance along fiber. We suspect, that the cable was sheared of the casing below the initial damage. Data recorded below 175 m is therefore discarded in the following.

During the cementation operation of the 18 5/8-inch anchor casing and 21-inch hole, an approximately 61 hours long DTS measurement was performed along the undamaged part of the MM fiber. The DTS measurement was started at 07:30 pm. Pumping of the cement slurry started approximately at 12:00 pm. The density of the cement slurry was

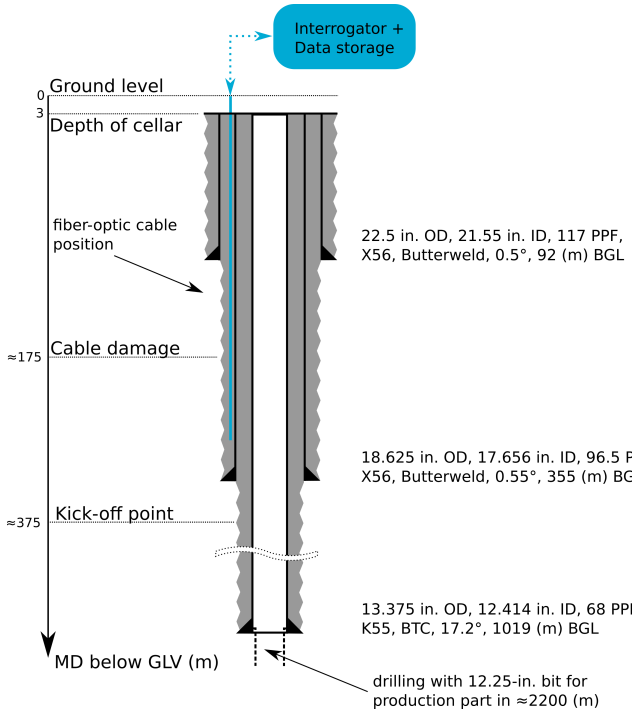

Fig. 1—Sketch of well RN-34 (not to scale) during the DAS measurement. The fiber-optic cable is illustrated in blue. Drilling for the 9 5/8-in. production liner commenced at approximately 2200 m depth

given as 1.7 g/cm^3. Primary cementation was carried out using a stinger. This was followed by a remedial top-up job. Cementation, including top-up jobs, was finished at approximately 10:00 am on the following day. After cementation and wait on cement (WOC) of approximately 25 hours, a cement bond log was run. The CBL tool was run in the 18-5/8-in anchor casing without surface pressure. After completion of the the CBL, operations were suspended for another 22 hours. DTS measurements continued for an additional 48 hours after completion of the cementing operations.

Subsequently, drilling commenced for the production casing down to 1019 m. The directional well trajectory was planed with a kick-off depth at 375 m, 1°/10 m built rate and an inclination of 17°. Once the production section was drilled, the 13 3/8-in. production casing was run to planned depth and cemented. Subsequently, the next 12 1/4-in. section was drilled to reach the reservoir interval for the installation of a 9 5/8-in. perforated production liner. During drilling and testing operations of the 12 1/4-in. section DAS data was continuously recorded for nine days. The final depth of well RN-34 was 2686 m

Data Acquisition The DTS data was recorded with a DTS Ultra system from Schlumberger. Data was acquired with a 0.5 m spatial resolution and a repetition rate of 37 s.

The DAS data was recorded along the second SM fiber with an iDAS unit by Silixa Ltd. Data recording started on 2015-03-17 01:37 pm and lasted until 2015-03-25 10:15 am (UTC time). Data was recorded with a sampling frequency of 1000 Hz, a 250 Hz low-pass filter, raw channel spacing of 25 cm, a gauge-length of 10 m, and stored in 1 min. long files. Prior to data analysis, noise adaptive, spatial down sampling was performed resulting in 1 m channel spacing.

Depth Correlation In order to relate individual fiber-optic channels along the optical cable to the physical position within the well, the ground level was determined by tapping the cable for the DAS data. Silixa Ltd. estimates the maximum error of this localization procedure be in the order of 2 m. For the DTS data, cold spray was used at the same location. Within the well, the cable is assumed to be straight down to 175 m.

Results

Cementation of the Anchor Casing

We start our analysis by investigating the temperature evolution during cementation of the anchor casing registered

along the MM fiber (**Fig. 2a**). The DTS data reveals an interval between 66 and 106 m depth (red dashed lines) where the temperature evolution, as measured by the fiber-optic cable, differs from the rest of the wellbore.

Before pumping of the cement slurry, about 7 hours after staring the DTS measurement, a temperature step is observed at 66 m depth. Constant temperature of around 10 °C is measured from 0 to 66 m. Below, temperatures around 15 °C are recorded. Below 66 m depth a thermal gradient is observed. Temperature gradually increases from 15 ° to around 20 °C at 175 m depth.

A temperature increase due to the arrival of the cement slurry is observed during primary cementation. The temperature signal rises up to the bottom of the aforementioned anomalous interval. Above 106 m depth the signal starts to fade, it vanishes at 100 m depth. Between 91 and 93 m depth an isolated, lower magnitude temperature increase is again observed. Above, again no temperatures signal from the cement slurry is observed up to 66 m depth. Above 66 m depth the temperature evolution commences as expected as the cement slurry rises close to the surface.

Cold water was then pumped through the annulus (at ≈12 h), as indicated by a sudden temperature decrease along the fiber-optic cable. Again, at 66 m depth the temperature as measured by the fiber-optic cable becomes discontinuous. Temperature abruptly rises from approximately 10 to 15 °C. Lower temperatures are again recorded between 82 and 92 m depth, similar to the reappearance of the temperature signal during pumping of the cement slurry.

Since the initially calculated cement volume was not sufficient for the slurry to reach the surface, two remedial top-up jobs were performed using 9 and 1 m^3 cement slurry respectively. This is seen in the data as small temperature increase close to the surface at approximately 13 hours after the start of the measurement.

Approximately 20 hours after the start of the measurement, we observe a temperature increase along the fiber-optic cable due to the exothermic hydration reaction of the cement slurry. The release of latent heat of hydration during cement setting lead to a temperature increase along the entire well. Between 82 and 92 m depth the released heat due to hydration is again higher than above and below, Maximum heat release is seen about 18 hours after finishing the primary cement job.

During drilling for the surface casing section, major circulation loss zones were identified in 41 and 85.5 m depth. During drilling operations for the anchor casing section no significant circulation losses occurred.

Fig. 2b shows the results of a caliper log run before installation of the anchor casing. The shoe of the surface casing is marked by the black dashed line. The loss of the temperature signal is preceded by a zone with considerable increases of the hole diameter.

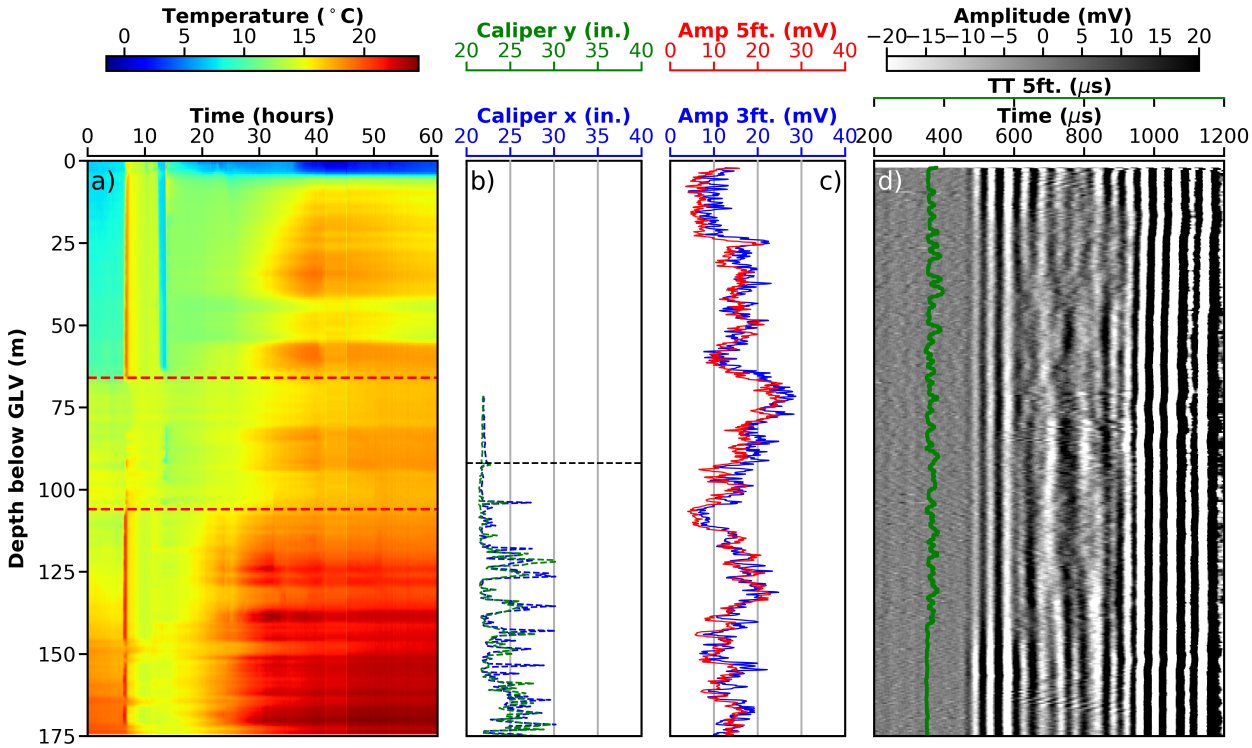

Fig. 2—DTS measurement and selected logs run in RN-34 during drilling and completing the anchor casing section. a) DTS temperature measurement. b) Caliper log. The black dashed line indicates the shoe of the surface casing at 92 m depth. c) CBL Amplitudes. d) Variable Density Log 5ft.

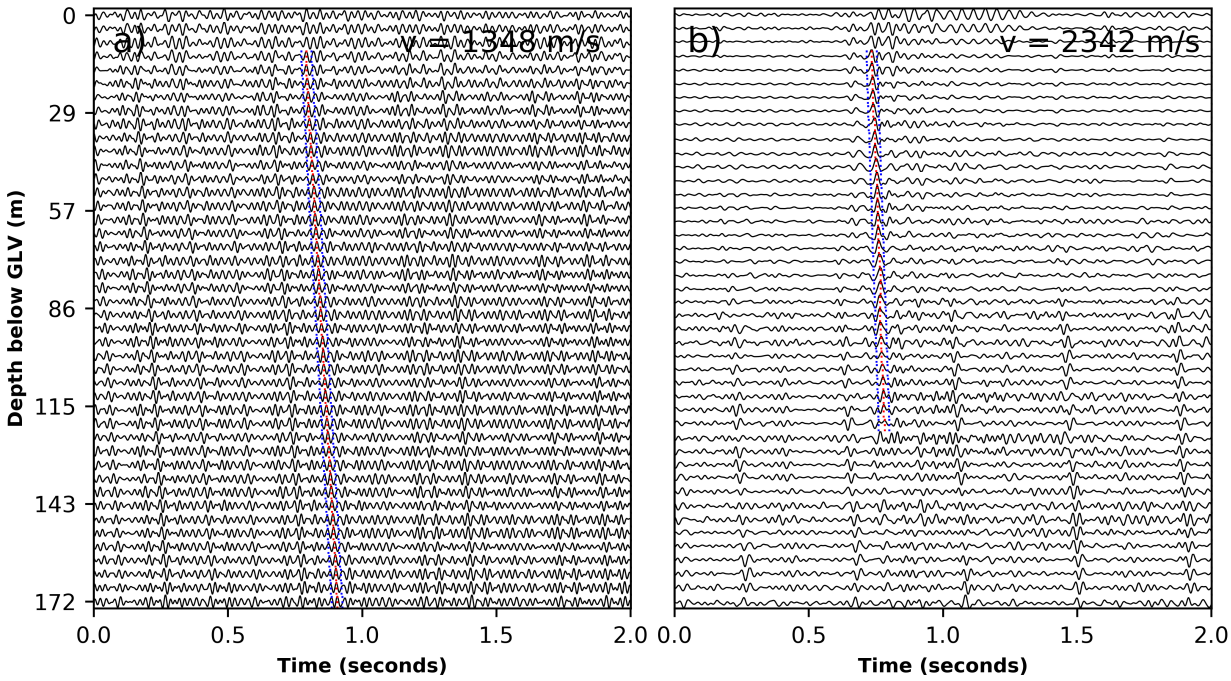

Fig. 3—Two seconds long data records containing exemplary wave types recorded during the DAS survey. Plotted is every fourth channel. a) Record start at 2015-03-21 03:00:47 am. Periodic signals with velocity of approximately 1348 m/s. b) Record start at 2015-03-23 11:31:45 am. Signal travelling at approximately 2342 m/s. Both signals have been picked as amplitude maxima (red lines) in moving time windows (blue lines).

Fig. 2c and d show the result of the conventional CBL performed within the anchor casing of well RN-34. 3 and 5ft. amplitudes are generally high. Low pipe amplitudes are only recorded in the topmost part of the casing, as well as a narrow interval around 100 m depth. Considerable casing arrivals are recorded in the VDL (5ft. spacing) over most of the depth profile. For clarity the travel time curve has been shifted by 100 μs, he travel time curve shows some cycle skipping, predominantly above 140 m depth. On site, drilling engineers concluded that a continuous cement column could be found behind the casing string. It was suspected that the cement had not properly set yet.

Dynamic Strain Signal Characteristic

Fig. 3 illustrates examples of signals recorded during the DAS survey, performed one and a half month after installation of the fiber-optic cable. Plotted is every fourth channel of the data record along the 18 5/8-inch anchor casing section. The data series for both examples have been detrended and integrated with respect to time, to convert them from strain-rate to stain. A 10 to 50 Hz Butterworth band-pass filter has been applied. Data plotted in Fig. 3a was recorded during injection testing of the reservoir. The flow rate was 113 l/s. Data shown in Fig. 3b was recorded after finishing the injection test with the drill string still out of hole.

The signals in both examples differ distinctively by their propagation velocity. Each signal was analyzed by picking the time and value of maximum amplitudes in a predefined moving window in space and time. From the picks, a linear regression was calculated to determine the average velocity. The signals in Fig. 3a travel with a speed of about 1348 m/s and appear to be periodic in time. The signal observed in Figure 3b travels at a significantly higher speed reaching approximately 2342 m/s and exhibits no periodicity.

Fig. 4 shows the picked maximum amplitudes versus depth of the aforementioned signals. The picking of the amplitude has been performed with the full data record, increasing the spatial density. The amplitude of the slower propagating signal (V=1348 m/s shown in Fig. 3a) shows an unsteady behaviour with sudden magnitude changes, e.g.,between 95 and 110 m depth. In contrast to the unsteady behaviour of the slower propagating signal, the amplitude of the faster propagating signal (V=2342 m/s shown in Fig. 3b) decays quadratically with depth. In addition the theoretical amplitude decay for a body wave as a result of spherical divergence is indicated by the blue dotted line in Fig. 4. Overall, the amplitude decay of the faster travelling signal closely follows the theoretical amplitude decay prediction. Between approximately 30 and 50 m depth, higher amplitudes are observed. This interval coincides with

	Drilling$_{T1}$	20 l/s injection$_{T1}$	113 l/s injection$_{T1}$	Drilling$_{T2}$	20 l/s injection$_{T2}$	113 l/s injection$_{T2}$
Position bit (m)	2210	out of hole	out of hole	2488	out of hole	out of hole
RPM (1/min)	62.3	0	0	62.3	0	0
Av. torque (dNm)	2789.6	0	0	3420.5	0	0
BOP	open	closed	closed	open	closed	closed
Mud pressure (bar)	115.4	23.0	74.1	104.1	25.9	73.7
Kill line pressure (bar)	0.8	16.9	37.3	0.7	19.5	34.6
Flow rate (l/s)	58.3	20.3	113.5	55.3	20.1	113.6

Table 1—Selected rig-log data for the three investigated activities. The subscript denotes the respective time window.

a depth interval showing higher amplitudes for the slower travelling signal.

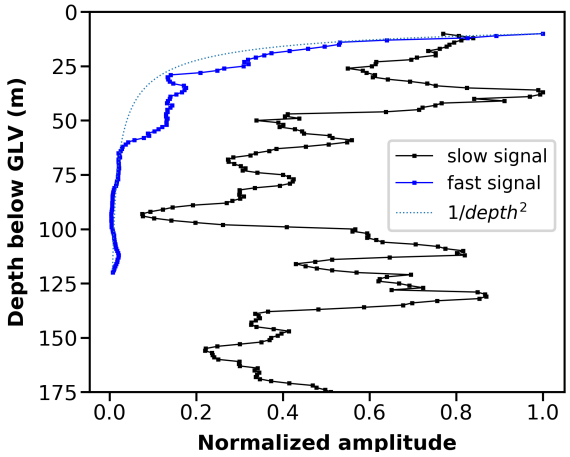

Fig. 4—Normalized maximum amplitudes for the signals from Fig. 3a (slow propagating signal) and Fig. 3b (fast propagating signal) against depth. The amplitude of the slower propagating signal (black) shows little attenuation correlated to depth. The amplitude of the fast propagating signal (blue) decays quadratically with depth (blue line), following the the theoretical prediction of the amplitude decay of body wave due to spherical divergence (blue dotted line).

Average Strain Amplitude Analysis

To estimate the relative, average strain amplitude transferred to the fiber-optic cable we calculate Root-Mean-Square values (RMS) for each channel in one minute long data files according to,

$$\mathrm{RMS} = \sqrt{\frac{1}{n}\sum_{i=1}^{n} x_i^2} \qquad (1)$$

where x_i is the strain-rate amplitude of the i'th sample in an n sample long time series.

Fig. 5(a-b) and **Fig. 6**(a-b) show twenty minutes of the aforementioned RMS values computed for three distinct activities during the survey: drilling, 20 and 113 l/s fluid injection respectively. For all three cases, computation has been carried out in two different time windows (Time window 1, Time window 2). **Table 1** summarizes averaged rig-log data for the corresponding time windows.

RMS-maps in the rows denoted by a) have been computed from raw data. For RMS-maps denoted by b) the raw data has been band-pass filtered between 30 and 60 Hz before computing the RMS values. The RMS maps have been normalized to a global maximum.

Injection testing was carried out for approximately 12 hours. Flow rates were alternated between 20 and 113 l/s each with a duration of approximately 45 minutes. Fluid injection was performed through the production casing, with the drill string out of hole.

For the drilling cases, time window 1 starts at 2015-03-18 11:40:07 am. Time window 2 starts at 2015-03-24 10:20:07 pm, approximately 6 days later. For the 20 l/s injection case time window 1 starts at 2015-03-21 02:00:07 am. Time window 2 starts at 2015-03-21 07:30:07 am, therefore separated by 5.5 hours. Likewise, for the 113 l/s injection

case time window 1 starts at 2015-03-21 01:00:07. Time window 2 starts at 2015-03-21 08:20:07. A separation of 7 hours and twenty minutes.

Starting times for the time windows have been selected arbitrary. The shorter time separation for the injection scenarios is due to limited duration of the injection test. During fluid injection, a very high vibrational load was observed close to the wellhead resulting in high RMS amplitudes for the first 25 m of the profile. To be able to compare the data measured during the different operations, the first 25 m of the RMS profile had to be excluded from the analysis.

The RMS-maps between the two time windows are generally similar and constant in time, except between the raw 20 l/s injection cases. For time window 1 no structural pattern is is apparent. For time window 2 the 20 l/s case is similar to 113 l/s injection case. We tested different band-pass filter widows to investigate if the same pattern could be revealed in some frequency interval. The frequency range between 30 and 60 Hz ultimately proofed most successful to increase the similarity between the two different cases.

Table 2 summarizes the average discrepancy between all combinations of RMS-maps from Fig. 5(a-b) and 6(a-b) according to,

$$\text{2D Discrepancy} = \frac{1}{nm}\sum_{i=1}^{nm}|x_i - y_i| \cdot 100 \quad (2)$$

where x_i, y_i are the individual pixel values of the RMS-map and $n \times m$ are the dimensions of the image. Generally the discrepancy is reduced by the filtering operation. Especially for the 20 l/s injection cases the discrepancy reduces from 26.2% to 7.9%.

Fig. 5c and 6c show amplitude spectra for the three cases from Fig. 5a and 6a. Frequency spectra have been computed from 10 s long time sections, located in the middle of the corresponding RMS time window. The frequency spectra have been normalized for each individual depth-channel. The three cases show distinct amplitude distributions. For the drilling case the energy is distributed evenly over the whole frequency range, whereas distinct frequency bands are excited during fluid injection. Between the two time windows the frequency spectra are again similar.

Fig. 7 illustrates the energy distribution for three channels located in 91 m (1 m before the shoe of the surface casing), 110 m and 125 m depth for the three analyzed cases. The amplitude spectra between the two time windows are again similar.

2D Discrepancy	drilling (1) raw	20 l/s (1) raw	113 l/s (1) raw	drilling (1) filt.	20 l/s (1) filt.	113 l/s (1) filt
drilling (2) raw	9.5 %	29.6 %	14.1 %	15.5 %	15.9 %	14.1 %
20 l/s (2) raw	11.6 %	26.2 %	7.7 %	18.3 %	11.1 %	7.6 %
113 l/s (2) raw	13.2 %	22.7 %	3.6 %	16.8 %	8.6 %	3.6 %
drilling (2) filt.	17.1 %	20.8 %	19.4 %	9.2 %	15.3 %	19.2 %
20 l/s (2) filt.	13.2 %	22.4 %	4.9 %	16.2 %	7.9 %	4.1 %
113 l/s (2) filt	13.3 %	22.2 %	3.9 %	16.4 %	8.1 %	3.3 %

Table 2—Discrepancy between the RMS-maps from Fig 5 and Fig 6. (1) and (2) indicate the two different time windows.

Drilling In Fig. 5(a-b) and 6(a-b), we observe a variable average strain amplitude with depth during drilling for both time widows. For the shallow part (<90 m) in the unfiltered case and time window 1 we observe elevated energy in 50, 70, and 85 m depth. For time window 2 elevated amplitudes are recorded in 55, 65, and 75 m depth. Maximum amplitudes are recorded between 120 to 125 m and around 135 m depth for both time windows.

For the band-pass filtered data (Fig. 5b and 6b) amplitude variation with depth is generally higher than for the unfiltered case. Amplitudes above 50 m are attenuated by the filtering operation. Contrary to the unfiltered case, dominate amplitudes are recorded in 65 and 75 m depth for both time windows. For time widow 1 significant (≈0.5) relative amplitudes are recorded at 45 m depth. Amplitudes between 12 and 125 m as well as around 130 m depth are reduced compared to the unfiltered case.

Generally the RMS profile is more or less constant in time. Relative amplitudes fluctuate between ≈0.6 and 1. Fluctuations in depth and time appear bigger for for time window 1 compared to time window 2. The frequency spectra (Fig. 5c and 6c) show high variability with depth. Constant frequency content is recorded close to the surface (<50 m), around 100 and 160 m depth. This indicates that the energy content for different frequencies is dependent on depth.

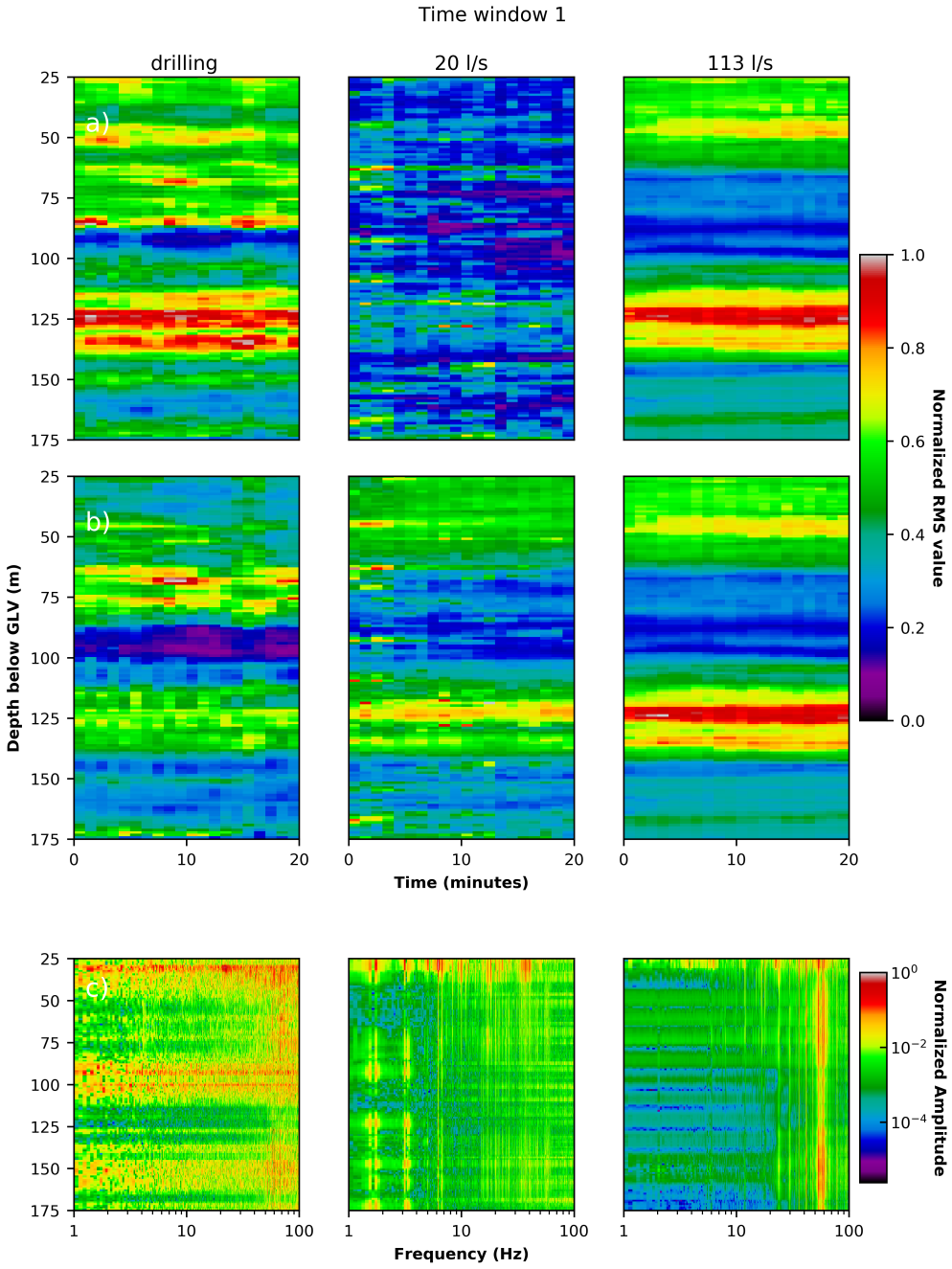

Fig. 5—(a-b) 20 minutes of RMS values of one minute long data records for distinct activities during the drilling operation in different frequency bands for time window 1. From left to right: drilling, 20 and 113 l/s fluid injection respectively. a) Unfiltered data. b) Band-pass filtered between 30 and 60 Hz. Left and right part of the figure have been calculated from different time widows in the continuous data set. c) Corresponding amplitude spectra computed from 10 s long time intervals.

Injection testing 20 l/s The largest discrepancy in the RMS-maps is observed between time window 1 and 2 in the unfiltered 20 l/S injection case (Fig. 5a and 6a). For time window 1 steady, low variability amplitude distribution, dominated by individual peaks, is observed. Time window 2 shows similar a amplitude distribution to the drilling case. Elevated amplitudes are recorded around 45 m, between 120 and 125 m, as well as around 130 m depth. The

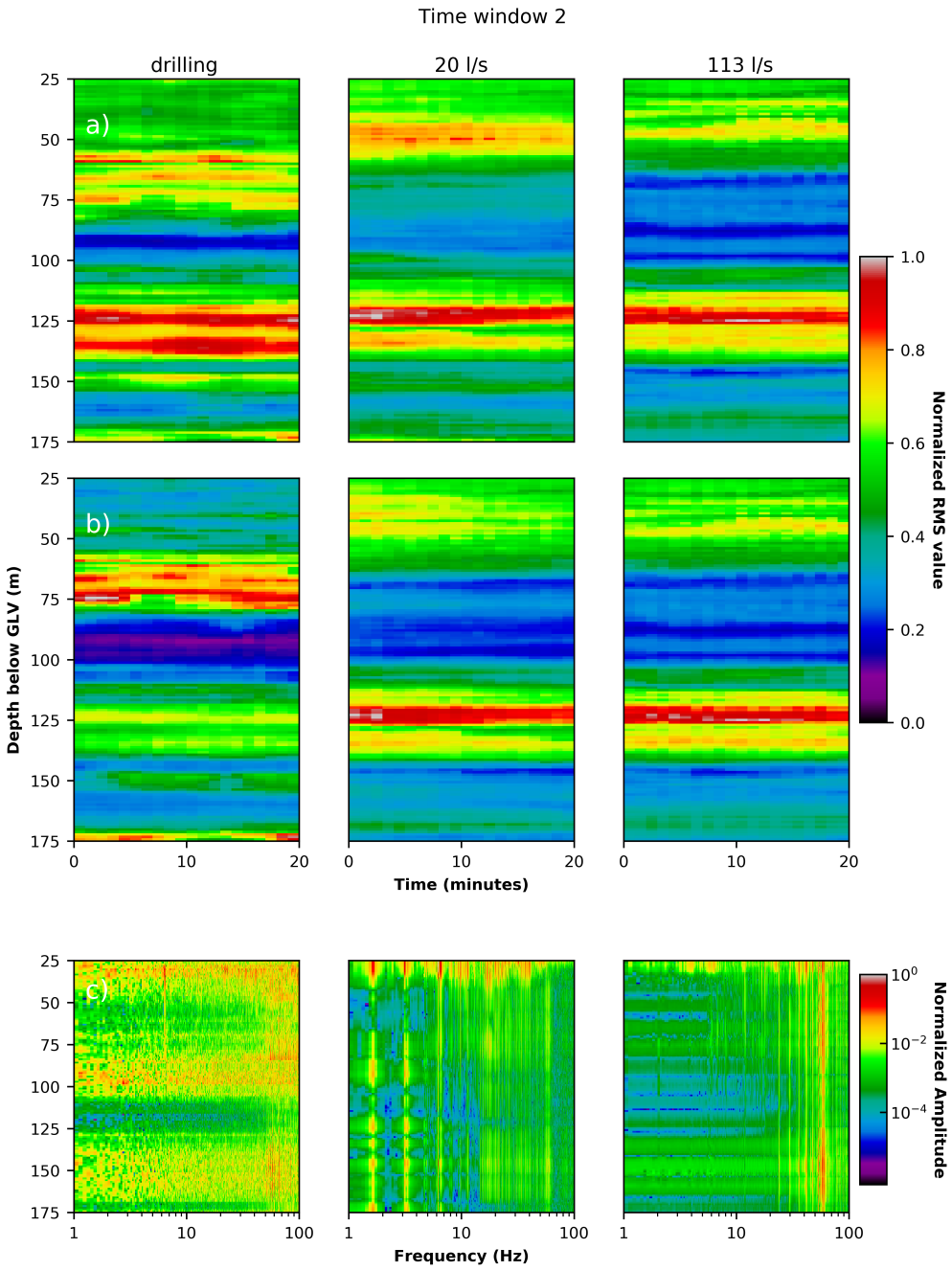

Fig. 6—(a-b) 20 minutes of RMS values of one minute long data records for distinct activities during the drilling operation in different frequency bands for time window 2. From left to right: drilling, 20 and 113 l/s fluid injection respectively. a) Unfiltered data. b) Band-pass filtered between 30 and 60 Hz. Left and right part of the figure have been calculated from different time widows in the continuous data set. c) Corresponding amplitude spectra computed from 10 s long time intervals.

frequency spectra in Fig. 5c and 6c shows elevated amplitudes in distinguished frequency bands between 1 and 10 Hz as well as close to 50 Hz.

For the band-pass filtered data (Fig. 5b and 6b), time window 2 shows little change compare to the unfiltered case. Relative amplitudes around 45 m depth reduce from around 0.9 to 0.7. The resolution is increased in that section. For

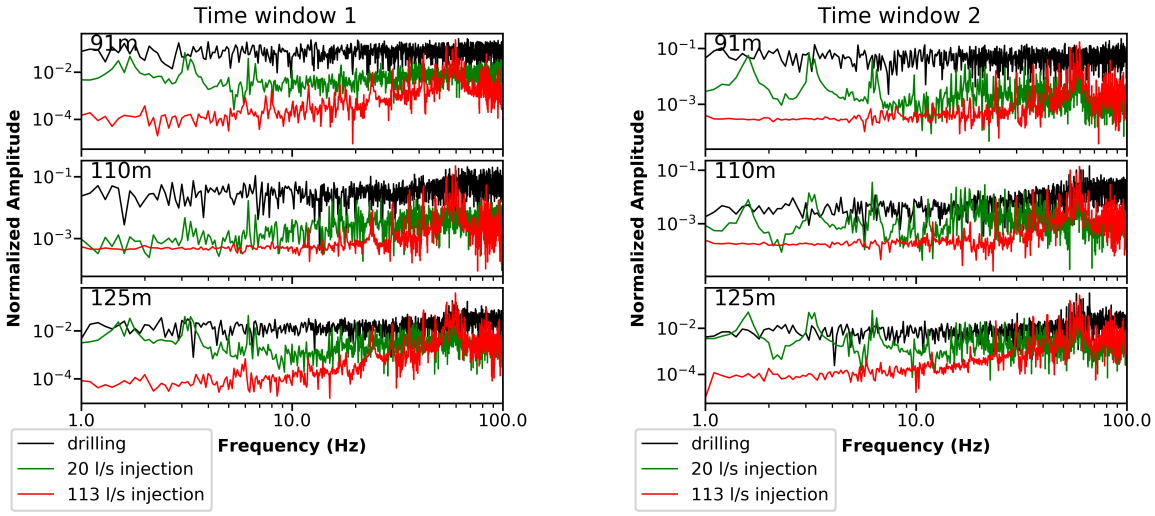

Fig. 7—Frequency spectra for three channels located in 91, 110, and 125 m depth for the three cases and two time windows from Fig. 5c and 6c.

time window 1, a significant change is observed. The amplitude distribution becomes similar compared to time window 2. Elevated amplitudes appear at 45, 125 and 130 m depth. Similarity to the drilling case is increased as well, except between 60 and 75 m depth. Here, both time windows show a low amplitude section, while maximum amplitudes are recorded for both the drilling case in both time windows. Again elevated amplitude sections are constant in time, with time window 2 showing less variability.

Injection testing 113 l/s For the 113 l/s injection case, variability is low between both time windows. Dominant amplitudes are recorded in the same depths as is the case with the drilling and 20 l/s injection case (125 and 130 m depth). The frequency spectrum is dominated by a strong signal around 60 Hz (Fig. 5c and 6c). As the spectrum is dominated by frequencies at 60 Hz, the bandpass filtered data between 30 Hz and 60 Hz does not differ much from the unfiltered data.

For all three operations, the average strain amplitudes calculated from 1 min. data remained mostly constant over the 20 min. that were analyzed. Time window 2 shows greater stability with time as well as depth. When comparing the average strain amplitudes for the three different cases, the main difference was found in the depth interval between 65 and 85 m, where higher amplitudes (>0.7) were observed for the drilling operation compared to lower values (<0.5) for both injection cases.

Comparison to CBL Data

Fig. 8a compares average strain amplitudes computed from two different time windows during drilling and testing the reservoir interval with conventional CBL data from Fig. 2c. A 20 min. normalized temporal mean from the 1 min. RMS values in the 30-60 Hz frequency range from Fig. 5b and 6b was calculated for all three cases. For the CBL data shown in Fig. 2c normalized amplitude was calculated for the interval between 25 and 175 m depth. CBL data was recorded with a spatial resolution of 0.1 m. To make it comparable to the one meter spaced DAS records the CBL amplitudes have been smoothed with a sliding average over 11 samples, centered at sample 6. Fig. 8b shows the difference between the 3ft. CBL- and mean RMS amplitude form Fig. 8a. For the difference computation, the 3ft. CBL data has been resampled to a spatial sampling of 1 m using the Fourier method.

Drilling For both time windows, when comparing the averaged strain amplitudes measured during the drilling phase with normalized CBL amplitudes, that overall similar trends with depth can be observed along the fiber-optic cable and in the CBL data although not all peaks match in both data sets. Time window 2 shows a larger offset at shallow depth. An additional peak is observed at 67 m depth. In the depth interval 75 to 85 m, the amplitude decrement along depth is stronger for the noise data from the drilling operation compared to the CBL amplitudes. Furthermore, the relative amplitudes from 85-100 m are lower for the average strain data. The maximum relative amplitudes during drilling were detected at the same depth as the maximum values for the CBL data at around 75 m and 125 m.

Injection testing 20 l/s The normalized average strain amplitudes measured during injection of 20 l/s again match the same trends as the average strain amplitudes generated during the drilling phase, although individual peaks have a different amplitude and slope with depth. A significantly different trend is again observed in the depth interval between 65 and 85 m, where average strain amplitudes remain low. Whereas the maximum average strain amplitudes during drilling are detected in the same depth as the maximum amplitudes for the CBL at about 75 m, maxima during fluid injection are observed around 125 m depth. Between time windows the data series remain similar

Injection testing 113 l/s For an increased injection rate, similar normalized average strain amplitudes were recorded with a higher amplitude interval close to 125 m depth and a low amplitude interval between 66 and 100 m depth. Overall, the normalized average amplitudes for the higher injection rate are slightly lower compared to the lower injection rate. This indicates a higher peak value. This is more prominent in time window 1.

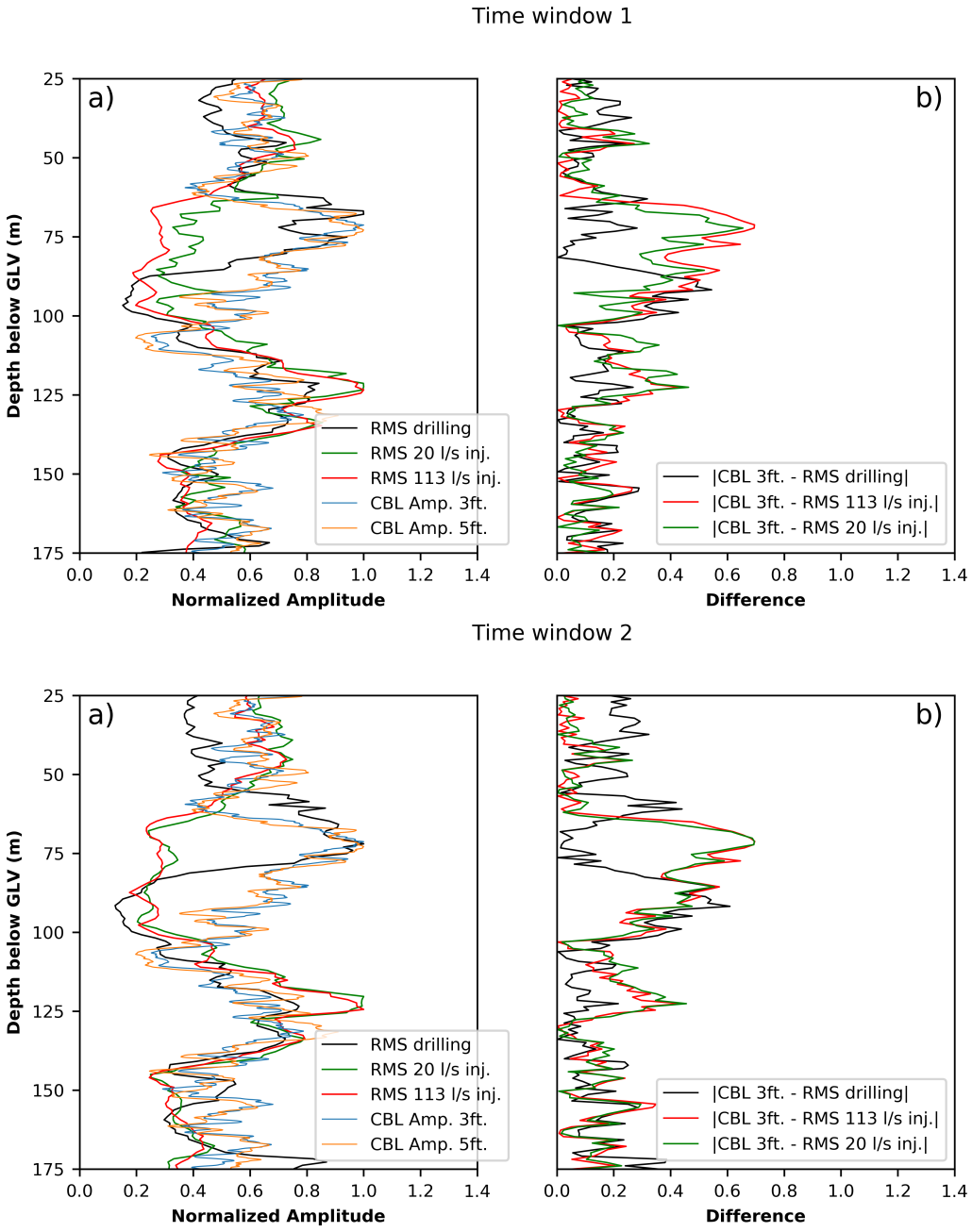

Fig. 8—a) Comparison between the temporal mean of the RMS values from Fig. 5b and 6b (30-60 Hz frequency range) for the three cases with conventional CBL amplitudes. All data series have been normalized. b) Difference between 3ft. CBL amplitude and mean RMS value.

In an attempt to quantify the similarity between the trends observed between the normalized CBL amplitudes and the normalized average strain amplitudes, a discrepancy was calculated according to Eq. 2 with $m = 1$, x_i, y_i are the individual data samples from the CBL as well as DAS data respectively. n is the number of data points with depth. The resulting data is plotted in **Table 3** and **Table 4**. Table 3 shows the average discrepancy for the whole depth profile which results in 15-20%. Table 4 shows the discrepancy for the interval below 100 m depth. For the interval below 100 m the error is in the order of 10-15%. Overall, data acquired during the drilling operation shows the highest similarity over the entire analyzed interval and below 100 m. Major differences are observed between 65 and 100 m depth, close to the shoe of the surface casing (92 m).

It is noteworthy that the difference between CBL amplitudes and the average RMS value against depth is again similar between the two different time windows.

1D Discrepancy	drilling (1)	20 l/s inj. (1)	113 l/s inj. (1)	CBL 3ft.	CBL 5ft
drilling (2)	9.2 %	20.3 %	20.2 %	18.3 %	18.4 %
20 l/s inj. (2)	15.4 %	7.5 %	3.3 %	21.1 %	20.6 %
113 l/s inj. (2)	15.1 %	9.6 %	3.0 %	20.8 %	20.0 %
CBL 3ft.	15.3 %	19.2 %	20.9 %	0.0 %	6.3 %
CBL 5ft	14.1 %	18.2 %	20.1 %	6.3 %	0.0 %

Table 3—Average discrepancy between average RMS- and CBL amplitudes form Fig 8. (1) and (2) indicate the two different time windows.

1D Discrepancy	drilling (1)	20 l/s inj. (1)	113 l/s inj. (1)	CBL 3ft.	CBL 5ft
drilling (2)	7.0 %	13.7 %	13.7 %	13.3 %	13.2 %
20 l/s inj. (2)	8.6 %	7.6 %	3.3 %	16.5 %	16.3 %
113 l/s inj. (2)	7.9 %	8.7 %	3.3 %	15.7 %	15.0 %
CBL 3ft.	13.1 %	15.3 %	15.7 %	0.0 %	7.0 %
CBL 5ft	11.8 %	14.2 %	14.8 %	7.0 %	0.0 %

Table 4—Average discrepancy between average RMS- and CBL amplitudes form Fig 8 below 100 m. (1) and (2) indicate the two different time windows.

Discussion

Similar trends have been observed for the normalized average strain amplitudes during drilling and injection testing compared to the normalized CBL amplitudes, the largest differences were observed in the interval between 66 and 106 m depth. This interval coincides with the depth interval where a different thermal signature along the optical cable was observed during cementation of the anchor casing. Therefore, first the DTS temperature information from the cementation will be discussed before the DAS data will be addressed.

Cementation of the Anchor Casing

Increasing temperatures measured along the optical cable indicate the presences of cement within the annulus behind the 18 5/8-in. anchor casing. Latent heat released during the hydration of the cement led to an overall increase of the temperature within the well and in the vicinity of the wellbore. Quickly increasing temperatures indicate a direct contact between cable and cement, slower increasing temperatures also indicate the presence of cement at depth. However, possible reasons are either the amount of cement in that depth is small, or there is little cement in the direct vicinity of the cable, the annulus at the position of the cable is thin or a combination of any of these aspects. A clear distinction cannot be made based on the available information.

The 18 5/8-in. anchor casing was cemented in two stages. For the primary cementation the flow of warm cement slurry in the vicinity of the cable can be observed. The positive temperature variation raises from bottom to top, indicating the continuous placement of cement in the annulus. In the interval from 66 to 106 m, the temperature variation due to flowing cement is smaller and between 66 and 85 m not observed at all. The bottom of this interval also corresponds the depth of increased borehole breakouts below the shoe of the surface casing at 92 m depth. At shallower depth (<66 m) the positive temperature variation is again observed, indication the presence of flowing cement around the cable.

Before remedial cementation, cold water was injected into the annulus. Although we see a strong temperature variation due to the presence of cold fluid flowing from the surface down to 66 m, only a smaller temperature variation was observed at greater depths. In addition, no temperature variation was observed at greater depths than 105 m.

After cold fluid injection, a top-up cementation was performed until the cement reached surface. A small temperature signature can be observed at shallower depth than 66 m. Again, the displacement from top to bottom can be confirmed by the temperature signature.

After cementation, temperature increased along the whole depth of the well due to the latent heat of cement during hydration. This indicates that cement is present in all depths. The magnitude of the temperature increase can typically be seen as a measure of the amount of cement per depth interval. It is typically higher in intervals of larger annular diameter compared to intervals with a narrower annulus.

Overall, the temperature evolution analyzed during primary and secondary cementation indicated that there seem to be less cement directly in the vicinity of the cable for the interval from 66 to 106 m. In addition, elevated CBL amplitudes in this interval indicate less cement bonding as well.

Dynamic Strain Signals

The two exemplary signal types with different propagation velocities and their relative recorded amplitudes in Fig. 3 and Fig. 4 were recorded during and shortly after injection testing. The measured DAS amplitude shown in Fig.3a therefore are likely caused by tube waves resulting from fluid injection into the wellbore. The speed of tube waves is related to mechanical fluid, well completion and formation properties. Their speed is typically slower than the speed of sound in water (see Norris 1989, for exemplary calculations), matching our observations. Since tube waves are guided by the well structure, no geometric attenuation is observed along the fiber-optic cable.

Because of the faster propagation velocity and quadratically decreasing amplitude, the signal from Fig. 3b is likely a compressional body wave resulting from some impact on the drill site. Whereas the source and its position is unknown, the amplitude decay with depth indicates a source close to the well. The signal energy is therefore transmitted across the formation and through cement sheet surrounding the fiber-optic cable.

The two waves mentioned above reach the fiber-optic cable from different directions (inside and outside), but show a similar trend at close to 50 m depth, this indicates that local strain amplitude variations are influenced by the coupling to and condition of the material surrounding the fiber-optic cable i.e. casing $\leftrightarrow$ cement $\leftrightarrow$ cable and formation $\leftrightarrow$ cement $\leftrightarrow$ cable.

Average Strain Amplitudes

The average strain amplitudes calculated for the three operations in different time windows show similar trends with depth, apart from the previously discussed interval between 66 and 106 m depth. It has to be stated, that the behaviour of the 20 l/s injection case in time widow 1 is not observed in other 20 l/s flow rate intervals during the injection test. Here, an additional noise source appears to be present, which can not be identified from the rig-log data. When filtering to appropriate frequency bands the discrepancy to time window 2 reduces to 7.9%. Assuming constant cable properties, locally changing properties of the medium surrounding the cable remain as the only explanation for the change in the average axial strain amplitudes recorded along the fiber-optic cable. Hence, the coupling between and mechanical properties of casing, cement and formation appear to determine the magnitude of the measured strain amplitudes. In the presented case, the signal source is located inside the well. Better coupling, leads to more effective energy transmission from inside the well to the formation, hence measured average signal amplitudes are lower. The lower the bonding, the more energy is trapped inside the well and the higher the measured amplitudes along the fiber-optic cable. The recorded signal amplitude behind casing, therefore, can potentially be used to monitor changing mechanical properties of the well completion and hence the integrity of the cemented annulus.

Comparison to CBL Data

In order to support the hypothesis that the average axial strain amplitude is a measure of the condition of the cemented annulus, the normalized average axial strain amplitude was compared to normalized amplitude values from a CBL log. Overall, both amplitudes show similar trends, although the CBL was logged during wait-on-cement and the noise log was acquired a month later after installation and cementation of the production casing. When calculating the discrepancy between both amplitudes we observed a high similarity between both data, especially in the drilling cases. When excluding the interval where we observed the temperature anomaly during the cementation, discrepancy is reduced from up to 21% to below 17% for the injection operations. For the strong noise source of the rotating drill string during drilling, we observed a reduction from about 18% to below 13%. The high similarity between both data indicates that the noise amplitude recorded along the fiber-optic cable is dependent on the material properties of the cemented annulus in a similar way than a conventional CBL tool. The similarity in the difference between CBL and average strain amplitudes between the two time windows suggest, that the measured average strain amplitude is influenced by other components of the well construction e.g. additional casing stings. Like for a conventional CBL, the measured amplitude is likely influenced by different parameters of the well construction e.g. the coupling strength

between different casing and cement sheets, as well as the formation or the compressional strength of the cement. Additionally, the measured CBL amplitude, as mentioned above, is influenced by a multitude of factors. Interpretation is therefore not always unambiguous. Especially the transition from open to cased hole and the presence of additional casing strings, as in our case above 92 m depth, is increasing the measurement uncertainty. The slurry density of 1.7 kg/cm^3 is unsuitable to explain elevated CBL amplitudes along the investigated depth interval. Below the shoe of the surface casing at 92 m depth, considerable washouts were recorded by the caliper tool, which might influence the CBL attenuation behaviour in that section. However, a clear correlation between elevated CBL amplitudes and wash-out zones is not observed.

High CBL amplitudes in the depth interval from 66 to 85 m indicate a lower cement bonding for this depth section. This coincides with the top of the observed temperature anomaly during cementation. Varying average strain amplitudes in this interval were observed during drilling and injection testing. In addition to the signal source, the wellbore pressure changed between both operations. Whereas the wellhead pressure during drilling was zero, 15 and 20 bar wellhead pressure was measured during injection testing with 20 and 113 l/s, respectively. The wellbore pressure increase might have resulted in an improved coupling between casing, cement and formation and hence a lower average axial amplitudes. The change in coupling as a result of pressure suggests non-optimal cement conditions in this depth interval. CBL data acquired without additional wellhead pressure on the other hand shows elevated amplitudes similar to the average axial strain amplitudes during drilling.

Conclusions and Outlook

From our analysis, we can draw the following conclusions:

- Distributed temperature sensing during cementation: The utilization of DTS data acquired during cementation of the anchor casing enabled us to study the cement placement. From the data it was possible to identify an interval with a different thermal signature during cementation. Temperature data suggests non-optimal cement placement. This interval also shows higher CBL amplitudes also pointing at non-optimal cement bonding.
- Real-time noise monitoring using distributed acoustic sensing: We analyzed passively recorded continuous average axial strain amplitudes acquired during different well operations and can conclude that the recorded signal amplitudes correlate with coupling properties of the well completion to the formation.

Further investigation is necessary to identify possible signal sources or increasing the fiber/interrogator sensitivity. In our case, drilling and injection testing provided sufficient signal energy to reveal information about the coupling condition of the well completion. The energy recorded during fluid circulation though the drill string or shut-in periods was not sufficient to reveal the information about the coupling properties. Although external signals as presented in Fig 3 were not analyzed in a greater detail, data suggests that sources from outside the wellbore can as well be used to analyze the coupling condition of the well completion.

Possible influencing factors, e.g. elastic parameters and additional cement sheets and casing strings, should be investigated. A mathematical model should be developed, incorporating the effects of changing well architecture.

It is established, that the reflection properties of optical fibers deteriorate over time due to the reaction of silicon dioxide with free hydrogen. For long term monitoring applications this issue would need to be addressed. Current proposals to overcome this problem include special carbon coatings and advanced glass compositions.

DTS succeeded in observing the cement placemen over the installation interval. This might offer a solution for investigation of low density, foam cements, which pose challenges for conventional cement evaluation tools.

It has been shown that the average axial strain amplitude recorded along an optical fiber is closely related to the coupling of the well completion to the formation. Hence, signal travelling along or through the well completion are more attenuated resulting in a lower average axial strain amplitude in case of good coupling conditions. This might also have an effect on the amount of signal energy that is trapped inside a well. The better the coupling, the lower the resulting signal energy inside the well. If this conclusion holds true, an assessment of the coupling condition of the well completion could also be made with DAS wireline or behind tubing installations opening the path to a wide implementation of this technology.

Given the ease of data acquisition, fiber-optic DAS measurements along a permanently installed fiber-optic cable behind casing are potentially suited, to monitor the long term coupling condition of the downhole completion. Hence, the mechanical integrity of a wellbore. A clear limitation of the DAS technology compared to conventional logging techniques is the channel spacing and the lack of radial resolution in the current implementation. Emerging distributed strain sensing technologies might be able to overcome the spatial sampling limitation of current DAS systems. The lack of radial resolution might be addressed by installing more than one fiber-optic cable or currently emerging cables that allow for the acquisition of three component data. Distributed fiber-optic sensing systems, however, will likely not

be able to match conventional sonic and ultrasonic well logging tools in resolution and precision. They are candidate technologies however to monitor the mechanical properties of the cemented annulus in real time over the entire life-cycle of a well. Real-time monitoring, thereby, will allow for analysing load cycles during production or injection, optimizing costly maintenance operation and ultimately ensure the longevity of downhole installations.

Acknowledgements

Data was acquired within the framework of project IMAGE (Integrated Methods for Advanced Geothermal Exploration), funded by the EC Seventh Framework Programme under grant agreement No. 608553.
This study has received funding from the European Union's Horizon 2020 research and innovation program under grant agreement No 654497 (GeoWell project). We would like to thank our partners from the GeoWell project for the excellent collaboration, constant support during data acquisition and analysis as well as the fruitful discussions over the past years. We are especially grateful to Árni Ragnarsson, Ingólfur Örn Þorbjornsson and Gunnar Skúlason Kaldal and their colleagues from ÍSOR as well as Guðmundur Ómar Friðleifsson and Ómar Sigurðsson and their colleagues from HS ORKA. We would like to thank Andi Clarke and his colleagues from Silixa Ltd. for their effort during data acquisition and analysis. At GFZ, we would like to thank David Bruhn, Ernst Huenges, Philippe Jousset, Christian Cunow, Jörg Schrötter, and Ronny Giese as well as all colleagues in section 4.8 Geoenergy who contributed to this project in one form or the other.

References

Bukhamsin, A. and Horne, R. 2016. Cointerpretation of Distributed Acoustic and Temperature Sensing for Improved Smart Well Inflow Profiling. Presented at the *SPE Western Regional Meeting* Anchorage, Alaska 23–26 May. SPE-180465-MS. https://doi.org/10.2118/180465-MS.

Dakin, J. P., Pratt, D. J., Bibby, G. W., et al. 1985. Distributed antistokes ratio thermometry. *Opt Fi Sens*. https://doi.org/10.1364/OFS.1985.PDS3.

Daley, T. M., Freifeld, B. M., Ajo-Franklin, J. B., et al. 2013. Field testing of fibre-optic distributed acoustic sensing (DAS) for subsurface seismic monitoring. *The Leading Edge* 32(6):699–706. https://doi.org/10.1190/tle32060699.1.

Davies, R. J., Almond, S., Ward, R. S., et al. 2014. Oil and gas wells and their integrity: Implications for shale and unconventional resource exploitation. *Mar. Pet. Geol.* 56:239–254. https://doi.org/10.1190/GEO2012-0444.1.

Dou, S., Lindsey, N., Wagner, A. M., et al. 2017. Distributed Acoustic Sensing for Seismic Monitoring of The Near Surface: A Traffic-Noise Interferometry Case Study. *Scientific Reports* 7. https://doi.org/10.1038/s41598-017-11986-4.

Förster, A., Schrötter, J., Merriam, D. F., et al. 1997. Application of opticalfiber temperature logging-An example in a sedimentary environment. *Geophysics* 62(4):1107–1113. https://doi.org/10.1190/1.1444211.

Goodwin, K. J. and Crook, R. J. 1992. Cement Sheath Stress Failure. *SPE Drill Eng* 7(4):291–296. https://doi.org/10.2118/20453-PA.

Götz, J., Lüth, S., Henninges, J., et al. 2018. Vertical Seismic Profiling using a daisychained deployment of fibre optic cables in four wells simultaneously – Case study at the Ketzin CO2 storage site. *Geophys. Prospect.* (online first). https://doi.org/10.1111/1365-2478.12638. URL https://onlinelibrary.wiley.com/doi/abs/10.1111/1365-2478.12638.

Grosmangin, M., Kokesh, P. P., and Majani, P. 1961. A Sonic Method for Analyzing the Quality of Cementation of Borehole Casings. *J Pet Tech* 13(2) SPE-1512-G-PA. https://doi.org/10.2118/1512-G-PA.

Hartog, A. H. *An Introduction to Distributed Optical Fibre Sensors*. Taylor & Francis Group 2017.

Hartog, A. H. and Leach, A. P. 1985. Distributed temperature sensing in solid core fibres. *Electronic Letters* 21(23): 1061–1062. https://doi.org/10.1049/el:19850752.

Hurtig, E., Schrötter, J., Großwig, S., et al. 1993. Borehole temperature measurements using distributed fibre optic sensing. *Scientific Drilling* 3(6):283–286. https://doi.org/10.13140/RG.2.1.3675.8567.

ISO/TS 16530-2. Well integrity – Part 2: Well integrity for the operational phase. ISO 2014. URL https://www.iso.org/standard/57056.html.

Jackson, R. B. 2014. The integrity of oil and gas wells. *Proc. Nat. Acad. Sci. U.S.A.* 111(30):10902–10903. https://doi.org/10.1073/pnas.1410786111.

Jousset, P., Reinsch, T., Ryberg, T., et al. 2018. Dynamic strain determination using fibre-optic cables allows imaging of seismological and structural features. *Nature Communications* 9 (in press).

Jutten, J. J., Quillot, D., and Parcevaux, P. A. 1989. Relationship Between Cement Slurry Composition, Mechanical Properties and Cement-Bond-Log. *SPE Production Engineering* 4(1):75–82 SPE-16652-PA. https://doi.org/10.2118/16652-PA.

Liu, X., Jin, B., Bai, Q., et al. 2016. Distributed Fiber-Optic Sensors for Vibration Detection. *Sensors* 16(8). https://doi.org/10.3390/s16081164.

Masoudi, A., Belal, M., and Newson, T. P. 2013. A distributed optical fibre dynamic strain sensor based on phase-OTDR. *Meas. Sci. Technol.* 24(8). https://doi.org/10.1088/0957-0233/24/8/085204.

Norris, A. N. 1989. The speed of tube waves. *J. Acoust. Soc. Am.* 87(1):414–416. https://doi.org/10.1121/1.399262.

Pardue, G. H., Morris, R. L., Gollwitzer, L. H., et al. 1963. Cement Bond Log-A Study of Cement And Casing Variables. *J Pet Tech* 15(5):545–555 SPE-453-PA. https://doi.org/10.2118/453-PA.

Parker, T., Shatalin, S., and Farhadiroushan, M. 2014. Distributed acoustic sensing - a new tool for seismic applications. *First Break* 32(2):61–69. https://doi.org/10.3997/1365-2397.2013034.

Reinsch, T. and Henninges, J. 2010. Temperature-dependent characterization of optical fibres for distributed temperature sensing in hot geothermal wells. *Meas. Sci. Technol.* 21(9):094022. https://doi.org/10.1088/0957-0233/21/9/094022. URL http://stacks.iop.org/0957-0233/21/i=9/a=094022.

Reinsch, T., Henninges, J., and Ásmundsson, R. 2013. Thermal, mechanical and chemical influences on the performence of optical fibres for distributed temperature sensing in a hot geothermal well. *Env. E. Sci.* 70(8):3465–3480. https://doi.org/10.1007/s12665-013-2248-8.

Reinsch, T., Thurley, T., and Joussen, P. 2017. On the mechanical coupling of a fiber optic cable used for distributed acoustic/vibration sensing applications–a theoretical consideration. *Meas. Sci. Technol.* 28(12). https://doi.org/10.1088/1361-6501/aa8ba4.

Song, R., Liu, J., Lv, X., et al. 2013. Effects of tool eccentralization on cement-bond-log measurements: Numerical and experimaental results. *Geophysics* 78(4). https://doi.org/10.1190/GEO2012-0444.1.

Southon, J. N. A. 2005. Geothermal Well Design, Construction and Failures. Presented at the *World Geothermal Congress* Antalya. Turkey 24–29 April. URL https://www.scopus.com/record/display.uri?eid=2-s2.0-84883389324&origin=inward.

Thiercelin, M. J., Dargaud, B., Baret, J. F., et al. 1998. Cement Design Based on Cement Mechanical Response. *SPE Drill & Comp* 13(4):266–273. https://doi.org/10.2118/52890-PA.

SI Metric Conversion Factors

°C+273.15	E+00=K
in. × 2.54*	E-02=m
ft. × 0.30	E+00=m
l/s	E-03=m^3/s
bar	E+05=Pa

*Conversion factor is exact

Tobias Raab works as an research associate at German Research Centre for Geosciences (GFZ). He holds a MS degree in applied geo-sciences from the Technical University of Berlin, specializing in geophysics. Research interests include seismology and scientific programming.

Thomas Reinsch is a research scientist at GFZ. He holds diploma degrees in physics and geology from the University of Cologne as well as a PhD in petroleum engineering from the Clausthal University of Technology.

Santiago Ruben Aldaz Cifuentes is a research scientist at GFZ and ICDP Potsdam, Germany. He holds a MS degree in petroleum engineering with special focus in drilling and production from the Technical University Clausthal, Zellerfeld and a ME degree in renewable energy systems from the Hamburg University of Applied Sciences.

Dr. Jan Henninges holds a PhD in the field of applied geophysics from the Technical University of Berlin. Since 2001 he is a research scientist at GFZ. His research interests include monitoring of dynamic subsurface processes, particularly applying fiber-optic sensing techniques in boreholes.